Smart Sensors to Reduce Pollutant Emissions in Transportation, Phase II

Center for Transportation, Environment, and Community Health
Final Report

by

Ramana Chintalapalle
Mallesham Bandi
Vishal Zade
Aldo Rubio
Ruey Long Cheu

The University of Texas at El Paso

March 31, 2020

DISCLAIMER

The contents of this report reflect the views of the authors, who are responsible for the facts and the accuracy of the information presented herein. This document is disseminated in the interest of information exchange. The report is funded, partially or entirely, by a grant from the U.S. Department of Transportation's University Transportation Centers Program. However, the U.S. Government assumes no liability for the contents or use thereof.

TECHNICAL REPORT STANDARD TITLE PAGE

1. Report No.	2.Government Accession No.	3. Recipient's Catalog No.
4. Title and Subtitle Smart Sensors to Reduce Pollutant Emissions in Transportation, Phase II		5. Report Date March 31, 2020 6. Performing Organization Code
7. Author(s) Ramana Chintalapalle, Mallesham Bandi, Vishal Zade, Aldo Rubio, Ruey Long Cheu		8. Performing Organization Report No.
9. Performing Organization Name and Address Center for Advanced Materials Research University of Texas at El Paso El Paso, TX 79968		10. Work Unit No. 11. Contract or Grant No. 69A3551747119
12. Sponsoring Agency Name and Address U.S. Department of Transportation 1200 New Jersey Avenue, SE Washington, DC 20590		13. Type of Report and Period Covered Final Report 10/1/2018 to 3/31/2020 14. Sponsoring Agency Code US-DOT

15. Supplementary Notes

16. Abstract

The proposed project is intended to design, develop, characterize, and demonstrate the feasibility of oxide materials based sensors, which are compatible for high temperature operation and efficient in functionality in a wide range of pressures that encountered in engines, for utilization in next generation, advanced transportation systems. The goal is to design and develop oxide sensing elements, evaluate their performance and demonstrate the relative merits of sensor elements based on hybrid nanostructures of economically viable materials for application in internal combustion engines of automotive industry. In this work, the Ba-Fe containing perovskites are engineered to serve the high-temperature and harsh environments of vehicle technologies while reducing the pollutant emissions. Doped perovskite materials exhibiting temperature independent conductivity has gained enormous attention for high temperature oxygen sensors due to great advantage over traditional doped metal oxides. This report focused on effect of sintering temperature on structure, morphology to explore correlation between oxygen sensing response of Ba(Fe0.7Ta0.3)O3-δ (BFTO30) bulk ceramics with structural and morphological features. Conventional solid-state reaction was used to synthesize BFTO30 powders. Crystal symmetry and phase purity of calcined and sintered powders was confirmed through X-ray diffraction analysis. Calcination of homogenous mixed precursors confirms that a single-phase perovskite phase without any secondary phases was obtained at 1150 °C. Samples were sintered at different temperatures (1200 °C, 1250 °C, 1300 °C, 1350 °C), X-ray diffraction of sintered samples reveals that there is a clear structural transformation from low symmetry rhombohedral to high symmetry cubic phase with temperature. Sintered samples exhibit porous morphological features with samples sintered at ≤1300 °C, whereas samples sintered at 1350 °C exhibits dense morphology with nearly spherical grains.

17. Key Words	18. Distribution Statement
Transportation, Sensors, Oxygen sensing, Sintering temperature, Mixed oxides, Solid state reaction	Public Access

19. Security Classif (of this report)	20. Security Classif. (of this page)	21. No of Pages	22. Price
Unclassified	Unclassified		

Form DOT F 1700.7 (8-69)

EXECUTIVE SUMMARY

The proposed project is intended to design, develop, characterize, and demonstrate the feasibility of oxide materials based sensors, which are compatible for high temperature operation and efficient in functionality in a wide range of pressures that encountered in engines, for utilization in next generation, advanced transportation systems. Specifically, the goal is to investigate the Ba-Fe containing perovskites to serve the high-temperature and harsh environments of vehicle technologies while reducing the pollutant emissions.

Perovskite oxides, which constitute wide range compositions, are earth-abundant and offer excellent means to realize chemical compounds, especially in the field of catalysis, that are economically viable and versatile in terms of technological or industrial applications. The advantages of perovskite structured ceramics (ABO_3) are high melting point, high decomposition temperatures, and dopant flexibility, allowing for changes in conductivity due to defects in their structure. The focus of this project is the perovskite structured Ba-Fe oxide doped with Ta with a composition $BaFe_{1-x}Ta_xO_{3-\delta}$ (BFTO30).

BFTO30 samples were synthesized using high-temperature, solid-state reaction method. Sintering temperature (1200-1350 °C) had an impact on the crystal structure and phase of BFTO30 ceramics. We observed structural phase transformation with increasing sintering temperatures. Samples sintered at 1300 °C and 1350 °C exhibit pseudo cubic perovskite structure, whereas samples sintered at 1200 °C and 1250 °C exhibit low symmetry phase. Scanning electron microscopy imaging analysis of the surface morphology indicate that BFTO30 samples sintered at 1200°C, 1250°C and 1300°C exhibit porous structure, while sample sintered at 1350°C exhibits a dense grain structure. The corresponding dielectric properties studies indicate that the dielectric constant and its relaxation time depend on the phase and microstructure of the BFTO30 ceramics. When correlating dielectric properties with morphology data, it can be observed that samples with higher surface porosity have a higher dielectric constant. Finally, in order to validate the sensor applications of BFTO, oxygen sensing measurements were carried out in a vacuum chamber. Samples were roughly polished and surface electroded using two-point measurement. A mixture of oxygen and argon gases at different concentrations in a temperature-controlled environment was used to evaluate electrical conductivity of BFTO30 differently sintered ceramics. BFTO30 sintered at 1300°C and tested at 500°C exhibits the shortest sensor response and recovery times.

TABLE OF CONTENTS

LIST OF FIGURES

1 INTRODUCTION

1.1 Problem Statement and Motivation

The proposed project is intended to design, develop, characterize, and demonstrate the feasibility of oxide materials based sensors, which are compatible for high temperature operation and efficient in functionality in a wide range of pressures that encountered in engines, for utilization in next generation, advanced transportation systems. The goal is to design and develop oxide sensing elements, evaluate their performance and demonstrate the relative merits of sensor elements based on hybrid nanostructures of economically viable materials for application in internal combustion engines of automotive industry. The hybrid multilayered nanostructures of Ba-Fe containing composites are expected to serve the high-temperature and harsh environments of vehicle technologies while reducing the pollutant emissions.

The innovations in transportation technologies, especially in the automobile industry, over the last few decades in conjunction with revolutionary trends in computing and information technologies have made our vehicles more powerful, easier to drive and control, safer, and energy efficient [1-3]. In fact, the modern vehicle for use in public and personal transportation is nothing but like a computer on wheels. With the aim of improving safety, fuel efficiency, and optimal utilization of roads, modern vehicles are being equipped with intelligent sensing, computation and communication technologies [2]. They employ a wide variety of sensors, which detect a variety of issues like tire pressure, acceleration, and engine oil quality, while also allowing controls for things like speed, temperature, power doors and power windows. Yet, when it comes to environmentally friendly nature, today's automobiles lack flexibility in design and contribute to the major portion of the environmental pollution. The problem is mainly with the design of engines and associated electronics and equipment.

In engines, controlling the combustion process through sensors and deriving the optimum conditions can eliminate the emission of environmental pollutants [3, 4]. Oxygen is present in certain ratio when a gasoline-powered engine burns gasoline. When there is less oxygen present, it is called a rich mixture and always fuel will remain after combustion. If there is more oxygen present it is referred to as a lean mixture. Operating under both the rich and lean mixtures are not good for the vehicle as well as for the environment [3, 4]. Running under fuel rich condition could cause not only environmental issues, but safety issues as well, due to the numerous amount of unburned fuel that could reignite inside the exhaust system. On the other hand, running the combustion process on the air rich range will generate higher amounts of NO_x (NO, NO_2) products that are the main contributors of acidic rain. This problem in vehicles can be addressed by means of oxygen sensors, which are typically positioned at near points in the exhaust system [3, 4]. The oxygen sensor creates a voltage due to a chemical reaction resulting from fuel to oxygen ratio. However, the oxygen sensors typically experience higher temperatures, where their functionality is limited and can eventually fail to operate. This is turn results in engines fail to function properly due to not able to determine the extent of combustion and air to fuel ratio. Furthermore, under such conditions, higher level of pollutant emissions will be released into the atmosphere. To address this fundamental issue, the proposed project is intended to design and develop novel sensors, which are temperature independent and smart. The proposed new generation sensors will take the

advantages of emerging nanotechnology into consideration to design and develop economically viable oxygen sensor element with a wider pO_2 ratio in the fuel compared to existing technologies. The technical merit of the project is based on the key idea of integrating the combined advantages of a wide bandgap oxide semiconductor with dopants to form a composite nano-structure, which can enable sensors that are mechanically robust and highly selective, sensitive for oxygen detection and monitoring. In addition, a hybrid, multilayered architecture is proposed to substantially elevate the operating temperature with excellent sensor performance.

1.2 Technical Merit and Significance

Perovskite oxides, which constitute wide range compositions, are earth-abundant and offer excellent means to realize chemical compounds, especially in the field of catalysis, that are economically viable and versatile in terms of technological or industrial applications [5-15]. The perovskite oxides find interesting applications in current and emerging electronics and electro-optics, electrochemical science and technology, electro-mechanical sensors and systems, solid oxide fuel cell technology, electromagnetic devices and magnetic tunnel junctions, and solid state memory device technologies. The perovskite oxide based piezoelectric materials are attractive for a number of applications in micromechanics, sensors, actuators, optoelectronics and energy harvesting applications [5-15]. Especially, the piezoelectric and ferroelectric properties, which often exists in the same perovskite oxide matrix, provide excellent means to harvest energy from multiple sources, which include mechanical, electrical, chemical, vibration and optical [13-15]. The dominance of oxide perovskites in the electro-mechanical and sensor technological applications and development is mostly due to their superior properties, such as high Curie temperature ($T_c \approx 390$ ℃), high dielectric constant (ε~20000 at T_c), low dielectric loss ($\tan \delta \sim 0.004$), and high piezoelectric coefficient ($d_{33} \sim 220$ pC/N) [15,16].

The crystal structure of a perovskite (ABO_3; Fig. 2) is named after the mineral perovskite $CaTiO_3$. The structure of an ideal perovskite consists of a cubic unit cell with an A-site species located at [½,½,½], B-site species at [0,0,0] and oxygen located at [½,0,0] resulting in the B-site species forming a sub-lattice of 6-coordinate, vertex-sharing octahedra and A-site species forming a sub-lattice of 12-coordinate face-sharing cuboctahedra [17, 18] (Fig. 2). However, the ideal perovskite cubic structure may be distorted depending on the size of the A and B cations. From structure point of view, the most notable feature is their versatility of accommodation. This primarily stems from flexible or adoptable structures that can be easily manipulated by means of doping various elements at the A- and B- sites of the perovskite structure (ABO_3).

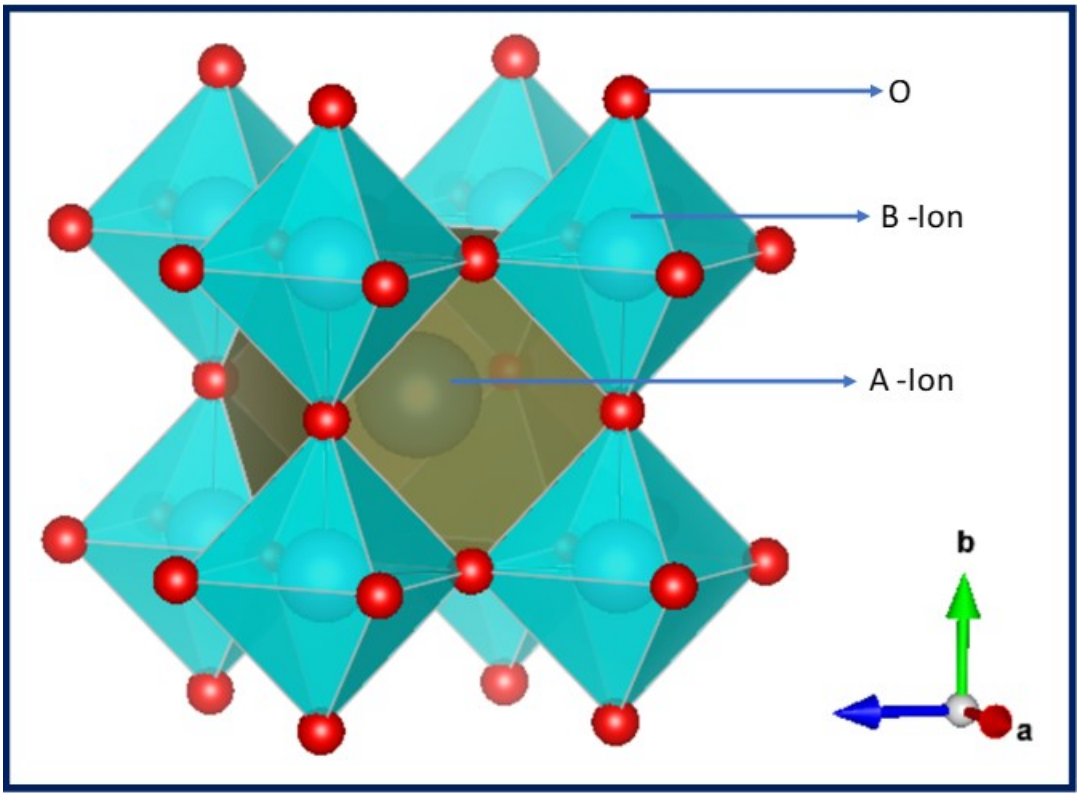

Figure 1 The ideal crystal structure of perovskite oxide with a general chemical formula of ABO3

Due to high melting point and decomposition temperature perovskite oxides are particularly attractive for high-temperature applications. High melting point and decomposition temperature of these materials provide microstructural and morphological stability to improve reliability and long-term sensor performance. Moreover, two differently-sized cations at A and B sites allow doping different elements and manipulate the properties and phenomena. Thus, flexibility of doping different elements allows to control the transport and catalytic properties, as consequence sensor performance is optimized for particular sensing application. Recently, the perovskite $Ba(Fe_{1-x}Ta_x)O_{3-\delta}$ (BFTO) has been reported as temperature independent oxygen sensor material over 400-900 ˚C temperature range. To the best of our knowledge there is not much literature of BFTO compounds. Thus, the challenging goal of the proposed project is to develop Ba-Fe containing perovskites and demonstrate their feasibility for oxygen sensors for utilization and direct integration into advanced transportation systems.

The specific objectives are as follows:

Objective 1: To synthesize and optimize $BaFe_xTa_{1-x}O_3$ with excellent control over architecture and morphology.

Objective 2: Evaluate the oxygen sensors for emission control and fuel efficiency in transportation systems.

Objective 3: To promote diversity and inclusiveness in research and education

The research tasks proposed include literature review, synthesis and characterization of Ba-Fe oxides, and oxygen sensor performance evaluation.

2 EXPERIMENTAL DETAILS

2.1 Synthesis

$Ba(Fe_{0.7}Ta_{0.3})O_{3-\delta}$ [BFTO30] compounds were synthesized using the conventional high-temperature solid-state chemical reaction method. High purity precursor materials, namely $BaCO_3$ (99.9%, Sigma Aldrich), Fe_2O_3 (99.9%, Sigma Aldrich) and Ta_2O_5 (99.9%, Sigma Aldrich), were weighed in stoichiometric proportion to achieve desired compound. Stoichiometrically weighed precursors homogeneously grounded in an agate mortar using acetone as wetting media. Homogeneously grounded powders were calcined at different temperatures (1000 °C, 1050 °C, 1100 °C and 1150 °C) with intermediate grinding to achieve phase purity. Calcined powders were re-grounded to decrease the particle size, fine powder was pelletized using a die and uniaxial hydraulic press by applying load of 1.5 ton in the form of circular disc (diameter – 8 mm and thickness - 1 mm). Pellets were sintered in a muffle furnace at a variable sintering temperature (T_s), which was varied in the range of 1200-1350 °C while the increment in temperature is set at 50 °C.

2.2 Characterization

X-ray Diffraction (XRD). X-ray diffraction (XRD) measurements were made using Rigaku X-ray diffractometer [Mini Flex II]. Both calcined and sintered compounds were analyzed at room temperature. The XRD parameters employed were: 10° – 80°(2θ range), step size – 0.02° and scan rate – 0.6°/min.

Rietveld Refinement Analysis (RA). The Rietveld refinement of experimental pattern carried using Fullprof Software. In Rietveld analysis, the peak profiles were defined using Thomson -Cox-Hastings (TCH) Pseudo -Voigt function, background was fitted using sixth order Chebyshev polynomial function. The Rietveld parameters such as; scale factor, zero correction, background, Full width half maximum/shape parameters, lattice parameters, position coordinates, occupancies and isothermal parameters were refined to achieve the satisfactory fit between experimental and simulated pattern. In order to refine the diffraction pattern, based on visual inspection, close structural models of $BaTiO_3$ based compounds were used. In Rietveld refinement choosing the right structural model which has an approximation to actual structure plays crucial role. Primarily the single-phase structural model was used refine the experimental pattern.

Transmission Electron Microscopy (TEM). The high resolution transmission electron microscopy **(**JEOL JEM-2100F TEM equipped with Oxford AZtec energy dispersive X-ray spectrometer and Gatan Tridiem GIF electron energy loss spectrometer) measurements were made to analyze the surface morphology and crystal symmetry of BFTO samples. Bright field images and selected area electron diffraction (SAED) patterns were recorded. All the measurements and imaging analysis is made on the BFTO samples prepared under variable synthetic conditions. In order to prepare TEM sample, a small amount of sintered powder was diluted with ethanol, suspension is sonicated, a single drop of the resulting suspension is placed onto a carbon-coated copper grid and allowed to dry in air.

2.3 Oxygen Sensor Testing and Evaluation

The sensor performance was evaluated in a test chamber. The electrical measurements were recorded using Keithley 6514 electrometer, and the input current was supplied via a Keithley 220 Programmable Current Source. Two gas tanks were employed for this investigation, a 99.99% Ar as the baseline gas, and a 99.99% O_2 as the analyte gas; both gasses were controlled using an MKS mass flow controller to achieve different partial pressures of oxygen. All the sensor performance responses were recorded as a function of synthetic conditions of the materials. The experiments were conducted at different oxygen pressures. Each pressure was subjected to 6 cycles (N=6) for repeatability. Each and every fitting procedure is carried out until the best fit (R is greater than 0.9 or better) is achieved.

Oxygen sensing measurements on the BFTO30 ceramic pellets were carried out in a vacuum chamber. The BFTO pellets were roughly polished and surface electroded using two-point measurement where contacts are supplied with 100 mA of DC current, while monitoring voltage drop in the sample. This surface two-point measurement electroding is commonly used in semiconductors rather than parallel plate electroding due to their relatively low conductivity at high temperatures. A mixture of oxygen (O_2) and argon gases was used to evaluate electrical conductivity of BFTO30 differently sintered ceramics in the form of two main sets of graphical data. System was brought to low vacuum before introducing gases in the chamber, and roughing pump was kept running to secure flow of gases. Argon gas was used as a baseline due to its inert nature to help desaturate sample pellets from oxygen gas (O_2). From preliminary testing, it was determined to do 10 minutes intervals of gas flow, changing from 100% argon gas flow to the various oxygen gas flow concentrations (20, 40, 60, 80%) in order to get cyclic conductivity readings. Resistance readings were taken every minute in real time using a recently developed new LabVIEW code. Measurements were taken at different, constant temperatures. Results were quantified to determine the sensor response, response time and recovery time.

3 RESULTS AND DISCUSSION

3.1 Crystal Structure and Phase Stability

X-ray diffraction patterns of $Ba(Fe_{0.7}Ta_{0.3})O_{3-\delta}$ compounds calcined at different temperatures (not shown here) reveal the presence of unreacted Ta_2O_5 secondary phase along with perovskite phase at lower calcination temperature (≤1100 °C). The complete solubility of precursors, formation single perovskite phase occurs only in samples calcined at 1150 °C for 8 h. The insolubility of Ta_2O_5 at lower calcination temperatures is attributed to its high melting point, which require relatively high calcination temperatures to decompose, stabilize into completely new structure. Figure 2 shows the XRD patterns of $Ba(Fe_{0.7}Ta_{0.3})O_{3-\delta}$ sintered at different temperatures. The peaks identified are as indexed It is evident that the BFTO samples stabilize in perovskite phase without any phase separation even at higher processing temperature. The crystallite size of all the BFTO samples sintered at different temperatures is estimated using Debye Scherrer relation:

$$D_{hkl} = \frac{0.9\lambda}{\beta \cos\theta} \quad (1)$$

where D is the crystallite size, λ ($Cu_{K\alpha}$)-1.5406 Å, β is the full width at half maximum, θ diffraction angle. The crystallite size increases from ~24 nm to ~80 nm with increasing T_s (1200-1350 °C).

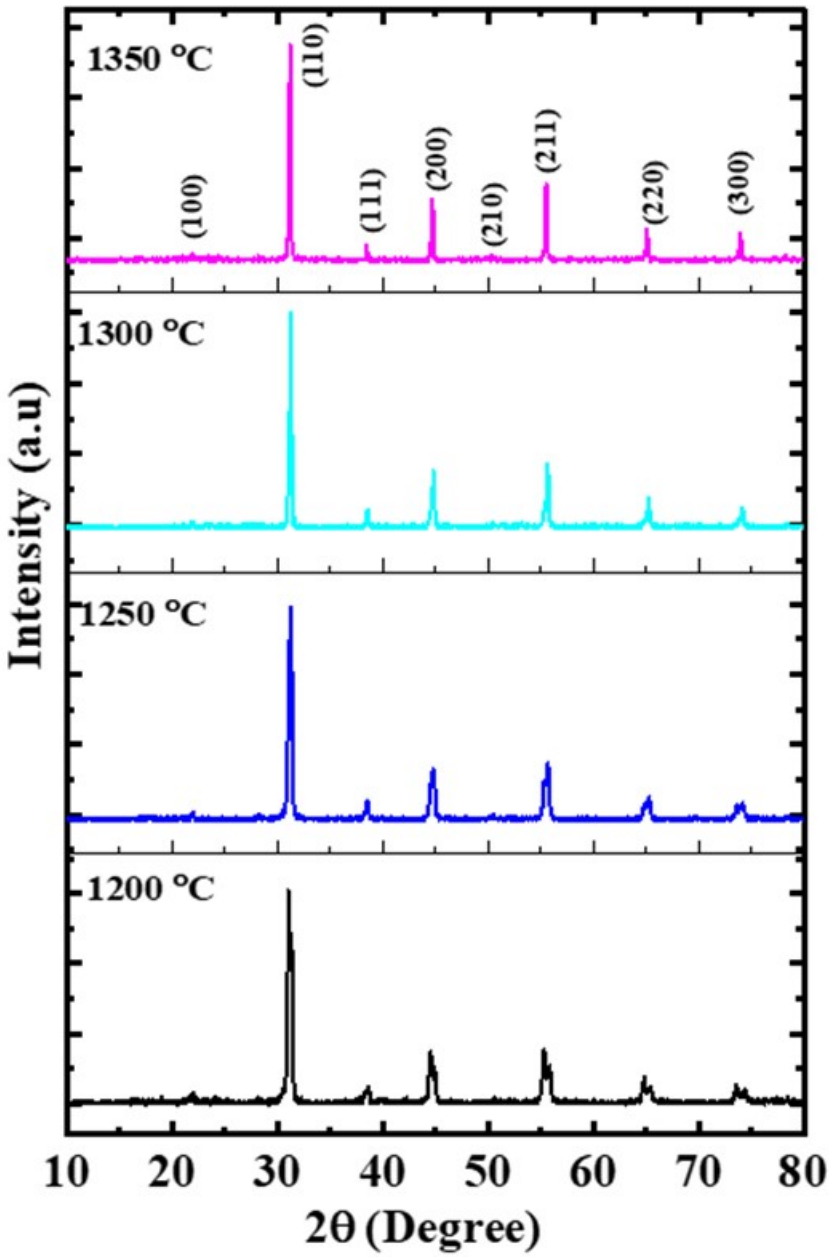

Figure 2 X-ray diffraction patterns of Ba(Fe0.7Ta0.3)O3-δ compounds sintered at different temperatures

The stability and symmetry of perovskite structure was determined by Goldschmidt tolerance factor (t)[36] based on the chemical formula given by:

$$t = \frac{R_A + R_O}{\sqrt{2}\,(R_B + R_O)} \quad (2)$$

where, R_A and R_B are the ionic radii of A site and B site cations, R_O is ionic radius of oxygen. The Shannon ionic radii[37] of constituent elements are: 1.61 Å (Ba^{2+}), 0.64Å (Ta^{5+}), 0.645Å (Fe^{3+}, high spin state), 0.55Å (Fe^{3+}, low spin state) and 1.4 Å (O^{2-}). The estimated tolerance factor values with Fe^{3+} high spin and low spin states are 1.07 and 1.11 respectively. From estimated tolerance factor value, it is evident that the synthesized BFTO compound might be stabilizing in hexagonal or tetragonal phase due to high difference between A site and B-site ionic radii.

Interestingly, a clear peak splitting is evident in the XRD of BFTO samples sintered at 1200 °C and 1250 °C. However, such peak splitting almost vanished in BFTO samples sintered at 1350 °C. The peak splitting nature is evident in the magnified reflections of (200), (211) and (220) reflections. For clarity and discussion of the crystal structure purpose, the magnified profiles of pseudo cubic $\{200\}_{PC}$ and $\{211\}_{PC}$ reflections are shown in Figure 3. Subscript PC indicates diffraction peaks are indexed using pseudo cubic symmetry. As can be noted in Fig. 4, variation in splitting feature and their intensity ratio with increasing T_s clearly evidence the structural transformations in BFTO30 with varying sintering temperature. All these reflections of BFTO samples sintered at 1200 °C exhibit doublet characteristics. At very first glance, splitting behavior of $\{200\}_{PC}$ reflection reveals tetragonal crystal symmetry, but for pure tetragonal phase intensity ratio of $I_{(002)}/I_{(200)}$ is ≈ 0.5 [(002) reflection correspond to lower Bragg angle, (200) reflection correspond to higher Bragg angle]. The observed intensity ratio between lower and higher Bragg angle peaks of $\{200\}_{PC}$ for BFTO sintered at 1200 °C is ≈ 1.6. This clearly rules out the tetragonal phase stability of BFTO samples sintered at 1200 °C. Moreover, for pure rhombohedral phase, (200) peak should be singlet, but observed doublet characteristics reveal absence of rhombohedral phase. However, the observed features of (200) reflection such as clear splitting and intensity ratio of $I_{(022)}/I_{(200)}$ is ≈ 1.6 are very similar to orthorhombic phase [20]. The broadening of $\{211\}_{PC}$ (which is also noted for $\{220\}_{PC}$) is attributed to presence of more than two peaks, which resulted from orthorhombic symmetry. Similar characteristic features of pseudo cubic reflections were also reported in doped-$BaTiO_3$ compounds, confirmed that the features associated with the resultant of mixed phases such as orthorhombic + rhombohedral or orthorhombic + tetragonal[15, 17, 20]. From preliminary peak analysis, it is evident that BFTO samples sintered at 1200 °C might be stabilizing in orthorhombic phase or mixed phase.

The BFTO samples sintered at 1250 °C showed a marked difference compared to those sintered at 1200 °C. Predominantly, distinct changes noted in XRD peak behavior for samples sintered at 1250 °C. The profiles of pseudo cubic reflections $\{200\}_{PC}$ and $\{211\}_{PC}$ exhibit reversal in the intensity of split peaks (Fig. 3). In addition to reversal in intensity, $\{200\}_{PC}$ reflection exhibits more distinct characteristics such as absence of clear splitting, in contrast to 1200 °C, and anomalous broadening with small shoulder peak at lower Bragg angle. These features evidence the structural transformation in BFTO30 with increasing sintering temperature. The reversal in the intensity of peaks with increasing sintering temperature from 1200 °C to 1250 °C may be attributed to the phase transition from orthorhombic to tetragonal structure [15, 20].

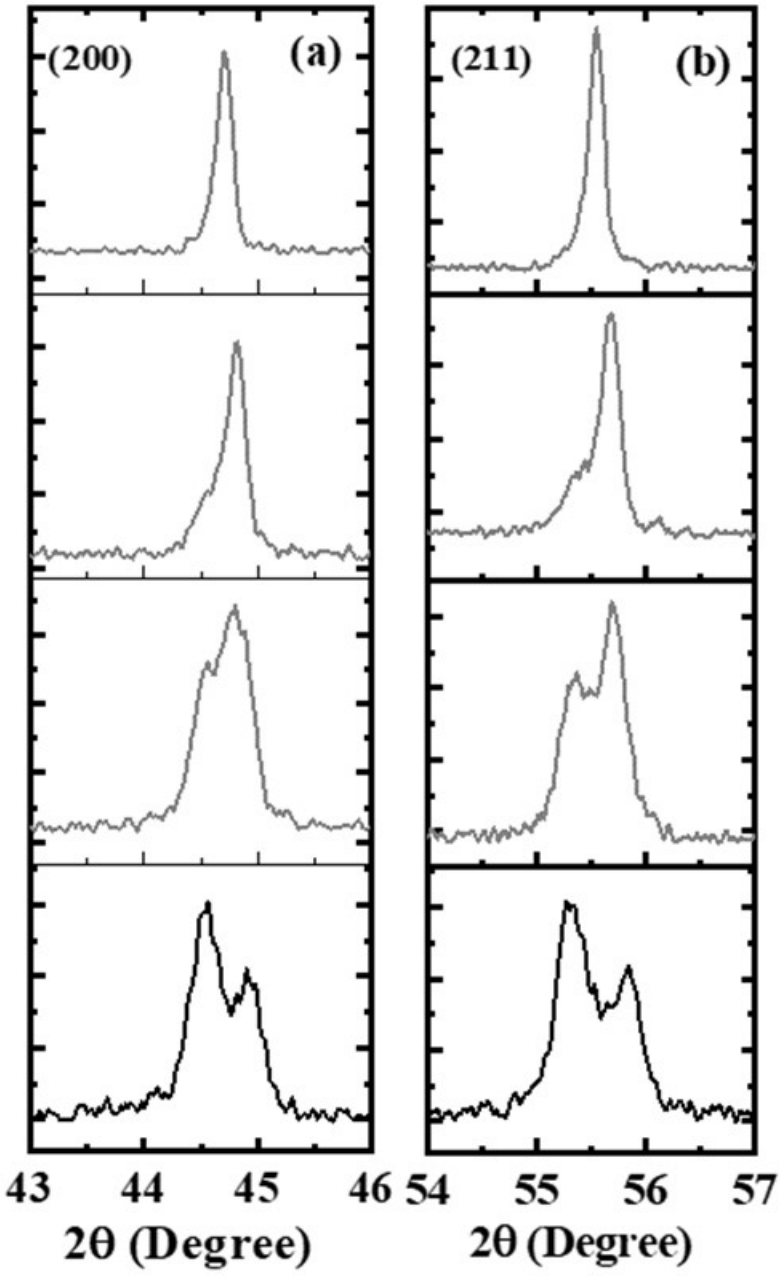

(a) {200}PC (b) {211}PC

Figure 3 Magnified pseudo cubic reflections of samples sintered at different temperatures

For BFTO samples sintered at 1300 °C, splitting of pseudo cubic reflections disappear, and peaks become highly asymmetric. For $\{200\}_{PC}$ reflection small shoulder at lower Bragg angle, broader shoulder for $\{211\}_{PC}$ reflections were observed. The noticeable changes between 1250 °C and 1300 °C can only be attributed to either structural transition or fraction of phase change. For BFTO samples sintered at 1350 °C, pseudo cubic reflections represented in Fig. 3 exhibit singlet

features. The singlet features of reflections at first glance reveals that the compound sintered at 1350 °C stabilizes in cubic phase. However, a deeper insight into reflections confirm that an asymmetry at lower Bragg angle along with singlet like features. These features might be attributed to stabilization of compound in rhombohedral phase (closest structure to cubic phase).

For BFTO samples sintered at 1350 °C, clear splitting of pseudo cubic reflections disappears, and peaks become highly asymmetric. For $\{200\}_{PC}$ reflection small shoulder at lower Bragg angle, broader shoulder for $\{211\}_{PC}$ reflection were observed. The noticeable changes between 1250 °C and 1300 °C are attributed to either structural transition or fraction of phase change. For BFTO samples sintered at 1350 °C, pseudo cubic reflections represented in Figure 3 exhibit singlet features. The singlet features of reflections at first glance reveals that the compound sintered at 1350 °C stabilizes in cubic phase. But, the deeper insight into reflections confirm that there is an asymmetry at lower Bragg angle along with singlet like features. These features might be attributed to stabilization of compound in rhombohedral phase (closest structure to cubic phase). Asymmetry in peaks may also associated with temperature induced strain or presence of smaller coherently scattered domain sizes.

3.2 Morphology and Microstructure

It is known that along with crystal structure and electronic structure, surface morphology will also play key role in gas sensing behavior of semiconductor oxides. Hence, it very important to know surface morphology of these ceramics to explore the best sintering temperature and optimized sensing behavior. Figure 4 shows the Scanning Electron Microscope (SEM) images of samples sintered at different temperatures. Samples sintered at 1200 °C, 1250 °C and 1300 °C exhibits porous structure varying porosity percentage, whereas samples sintered at 1350 °C exhibits close packed grains with nearly spherical shape. We also estimated the porosity of these samples using ImageJ; the estimated porosity of these samples includes: ≈ 14%, ≈ 4%, ≈ 7% and ≈ 1% respectively with increasing sintering temperature.

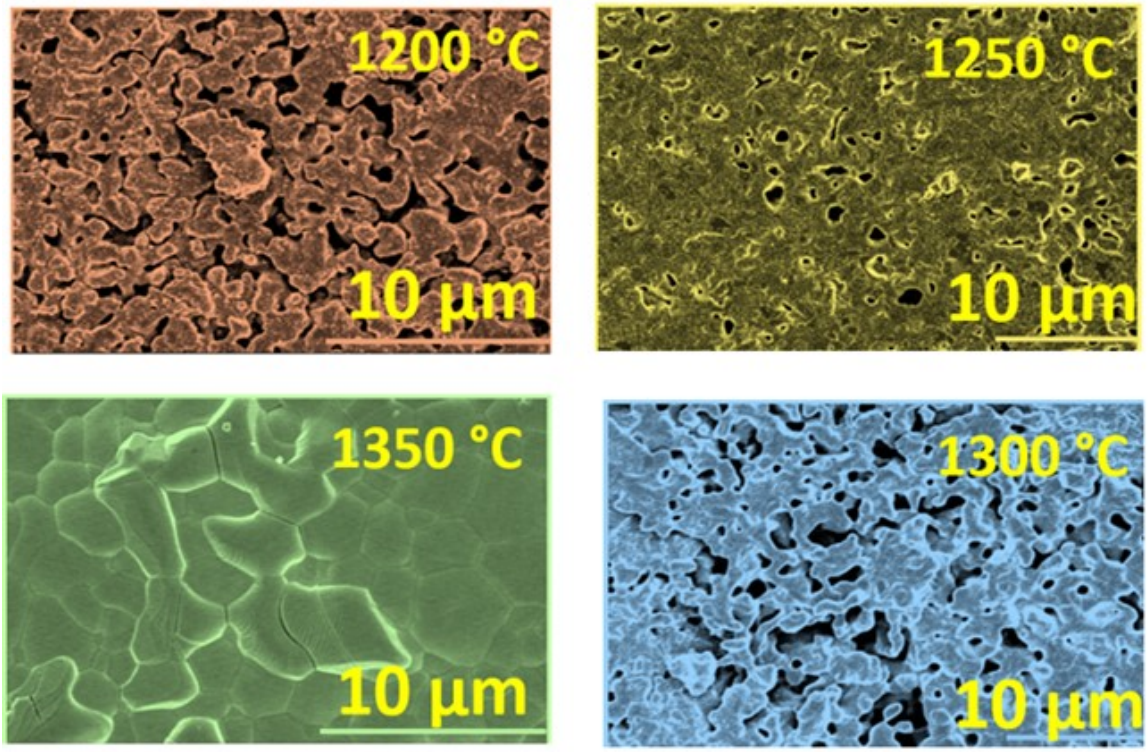

Figure 4 SEM images of BaFe0.7Ta0.3O3-δ sintered at different temperatures

3.3 Oxygen Sensor Performance

The temperature dependent electrical data, which serves the baseline characteristics for sensor applications, of BFTO samples are shown in Figure 5. It is generally accepted that barrier formation between grains is responsible for the sensor conductivity and that these barriers have a Schottky-type nature. Therefore, as a first step, determination of electrical characteristics as a function of temperature is quite important for utilization of BFTO for sensor applications. The temperature-dependent electrical data (Figure 5; Arrhenius plots) of BFTO samples were analyzed using the relation:

$$\sigma = \sigma_{\infty} e^{(\frac{E_A}{kT})} \quad (3)$$

where σ_{∞} is the conductivity at infinite temperature, E_A is the activation energy, k is the Boltzmann constant, T is the absolute temperature, and σ is the electrical conductivity of the BFTO sample. The data shown in Figure 5 are the plots of conductivity vs. temperature of BFTO30 samples sintered 1250°C and 1300°C and tested at constant 20% and 60% oxygen gas flow. From this figure, it can be observed that 1300°C sintered sample shows minimum change in the conductivity of one unit in the range of 400 - 700°C for both oxygen percentages. On the other hand, 1250°C sintered sample exhibits a higher change in the log of conductivity of around 1.2 units.

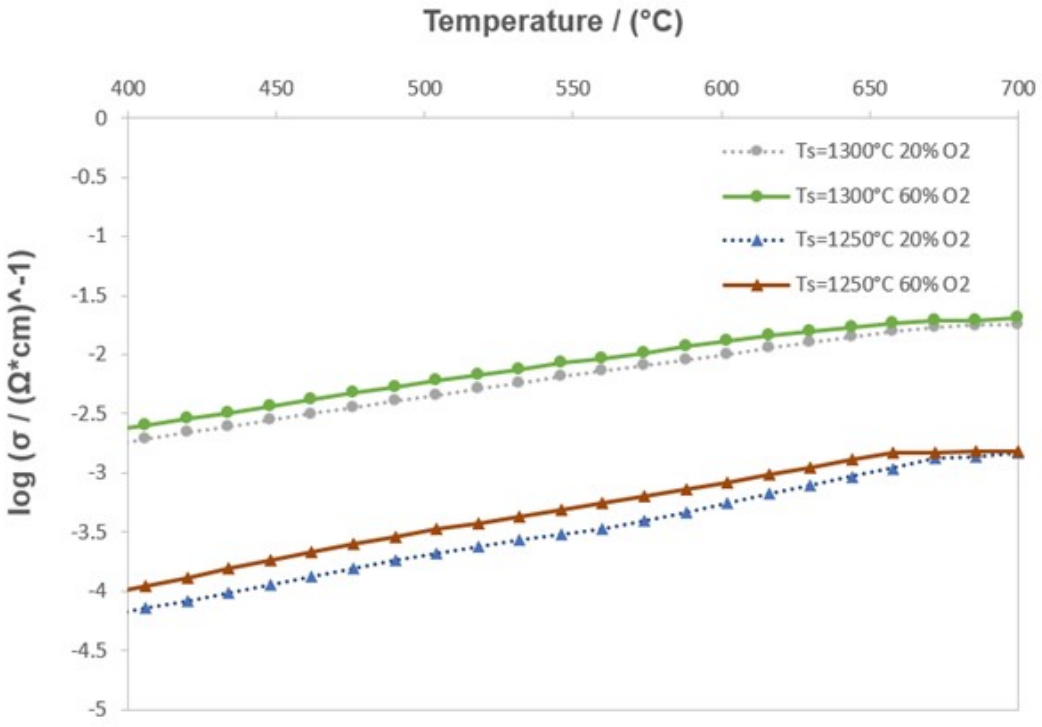

Figure 5 Plot of conductivity vs. temperature of BFTO30 samples sintered at 1250°C and 1300°C

4 SUMMARY AND CONCLUSIONS

$Ba(Fe_{0.7}Ta_{0.3})O_{3-\delta}$ compounds were synthesized using conventional solid state reaction route by varying the sintering temperature (1200 °C, 1250 °C, 1300 °C & 1350 °C). The effect of sintering temperature was significant on the crystal structure, phase stabilization and chemical quality of the resulting BFTO compounds. X-ray diffraction analyses reveal the evidence of structural transformations in BFTO with increasing sintering temperature. Detailed Rietveld analysis of the BFTO samples was performed using various closest structural models. The results of the present work suggest that the crystal structure, phase and chemical quality of the BFTO compounds can be controlled by simply tuning the processing temperature. The high chemical quality of these compounds. The fundamental understanding of the structure, phase and chemistry of $Ba(Fe_{0.7}Ta_{0.3})O_{3-\delta}$ compounds may be useful to develop optimized solid-state gas sensors based on $Ba(Fe_{0.7}Ta_{0.3})O_{3-\delta}$ ceramics. The preliminary testing of the selected BFTO compounds suggest their potential application in the design and development of high temperature oxygen sensors for utilization in transportation systems.

REFERENCES

1. Tewolde, G. S., 2012. Sensor and Network Technology for Intelligent Transportation Systems, Proceedings of 2012 IEEE International Conference on Electro/Information Technology, 1-7.
2. Mitchell, W. J., Borroni-Bird, C. E. and Burns, L. D., 2010. Reinventing the Automobile – Personal Urban Mobility for the 21st Century. The MIT Press.
3. Rubio, E. J., 2016. Intrinsic and Metal-Doped Gallium Oxide-Based High-Temperature Oxygen Sensors for Combustion Processes. Ph.D. Dissertation, The University of Texas at El Paso.
4. Yokogawa, 2008. Carbon Monoxide Measurement in Coal-Fired Power Boilers. file:///C:/Users/User/AppData/Local/Temp/TDLS_A_001.us-1.pdf.
5. Hong, W. T., Risch, M., Stoerzinger, K. A., Grimaud, A., Suntivich, J. and Shao-Horn, Y., 2015. Toward the Rational Design of Non-Precious Transition Metal Oxides for Oxygen Electrocatalysis. Energy & Environmental Science, 8, 1404-1427.
6. Hadri, A. E., Gómez-Recio, I., Río, E. D., Hernández-Garrido, J. C., Cortés-Gil, R., Hernando, M., Varela, A. U., Gutiérrez-Alonso, A. N., Parras, M. and Delgado, J. J., 2017. Critical Influence of Redox Pretreatments on the Co Oxidation Activity of $BaFeO_{3-\delta}$ Perovskites: An in-Depth Atomic-Scale Analysis by Aberration-Corrected and in Situ Diffraction Techniques. ACS Catalysis, 7, 8653-8663.
7. Seo, M. H., Park, H. W., Lee, D. U., Park, M. G. and Chen, Z., 2015. Design of Highly Active Perovskite Oxides for Oxygen Evolution Reaction by Combining Experimental and Ab Initio Studies. ACS Catalysis, 5, 4337-4344.
8. May, K. J., Carlton, C. E., Stoerzinger, K. A., Risch, M., Suntivich, J., Lee, Y.-L., Grimaud, A. and Shao-Horn, Y., 2012. Influence of Oxygen Evolution During Water Oxidation on the Surface of Perovskite Oxide Catalysts. The Journal of Physical Chemistry Letters, 3, 3264-3270.
9. Suntivich, J., Gasteiger, H. A., Yabuuchi, N., Nakanishi, H., Goodenough, J. B. and Shao-Horn, Y., 2011. Design Principles for Oxygen-Reduction Activity on Perovskite Oxide Catalysts for Fuel Cells and Metal–Air Batteries. Nature Chemistry, 3, 546-550.
10. Li, M., Pietrowski, M. J., De Souza, R. A., Zhang, H., Reaney, I. M., Cook, S. N., Kilner, J. A. and Sinclair, D. C., 2013. A Family of Oxide Ion Conductors Based on the Ferroelectric Perovskite $Na_{0.5}Bi_{0.5}TiO_3$, Nature Materials, 13, 31-35.
11. She, S., Yu, J., Tang, W., Zhu, Y., Chen, Y., Sunarso, J., Zhou, W. and Shao, Z., 2018. Systematic Study of Oxygen Evolution Activity and Stability on $La_{1-x}Sr_xFeO_{3-\delta}$ Perovskite Electrocatalysts in Alkaline Media. ACS Applied Materials & Interfaces, 10, 11715-11721.
12. Tripkovic, V., Hansen, H. A., Garcia-Lastra, J. M., and Vegge, T., 2018. Comparative DFT+ U and Hse Study of the Oxygen Evolution Electrocatalysis on Perovskite Oxides. The Journal of Physical Chemistry C, 122, 1135-1147.
13. Di Tommaso, S., Giannici, F., Marculescu, M. A., Martorana, A., Adamo, C. and Labat, F., 2014. Toward Tailorable Surfaces: A Combined Theoretical and Experimental Study of Lanthanum Niobate Layered Perovskites. The Journal of Chemical Physics, 141, 024704.
14. Keswani, B. C., Devan, R. S., Kambale, R. C., James, A. R., Manandhar, S., Kolekar, Y. D. and Ramana, C. V., 2018. Correlation between Structural, Magnetic and Ferroelectric Properties of Fe-Doped (Ba-Ca)TiO_3 Lead-free Piezoelectric. Journal of Alloys and Compounds, 712, 320-333.

15. Keswani, B. C., Patil, S., James, A., Kolekar, Y. and Ramana, C. V., 2018. Correlation between Structural, Ferroelectric, Piezoelectric and Dielectric Properties of $Ba_{0.7}Ca_{0.3}TiO_{3-X}BaTi_{0.8}Zr_{0.2}O_3$ (X= 0.45, 0.55) Ceramics. Ceramics International, 44, 20921-20928.
16. Panda, P., 2009. Environmental Friendly Lead-Free Piezoelectric Materials. Journal of Materials Science, 44, 5049-5062.
17. Zhou, H. and Goodenough, J. B., 2004. Polaron Morphologies in $SrFe_{1-x}Ti_xO_{3-\delta}$. Journal of Solid State Chemistry, 177, 1952-1957.
18. Wang, X., Wu, J., Xiao, D., Zhu, J., Cheng, X., Zheng, T., Zhang, B., Lou, X. and Wang, X., 2014. Giant Piezoelectricity in Potassium–Sodium Niobate Lead-Free Ceramics. Journal of the American Chemical Society, 136, 2905-2910.
19. Liu, X. C., Hong, R. and Tian, C., 2009. Tolerance Factor and the Stability Discussion of ABO_3-Type Ilmenite. J. Mater. Sci. Mater. Electron, 20, 323–327.
20. Dwivedi, S., Pareek, T. and Kumar, S. 2018. Structure, Dielectric, and Piezoelectric Properties of $K_{0.5}Na_{0.5}NbO_3$-Based Lead-Free Ceramics. RSC Adv., 8, 24286–24296.